



An EOF-based observing system design for a tropical Indian Ocean mooring array

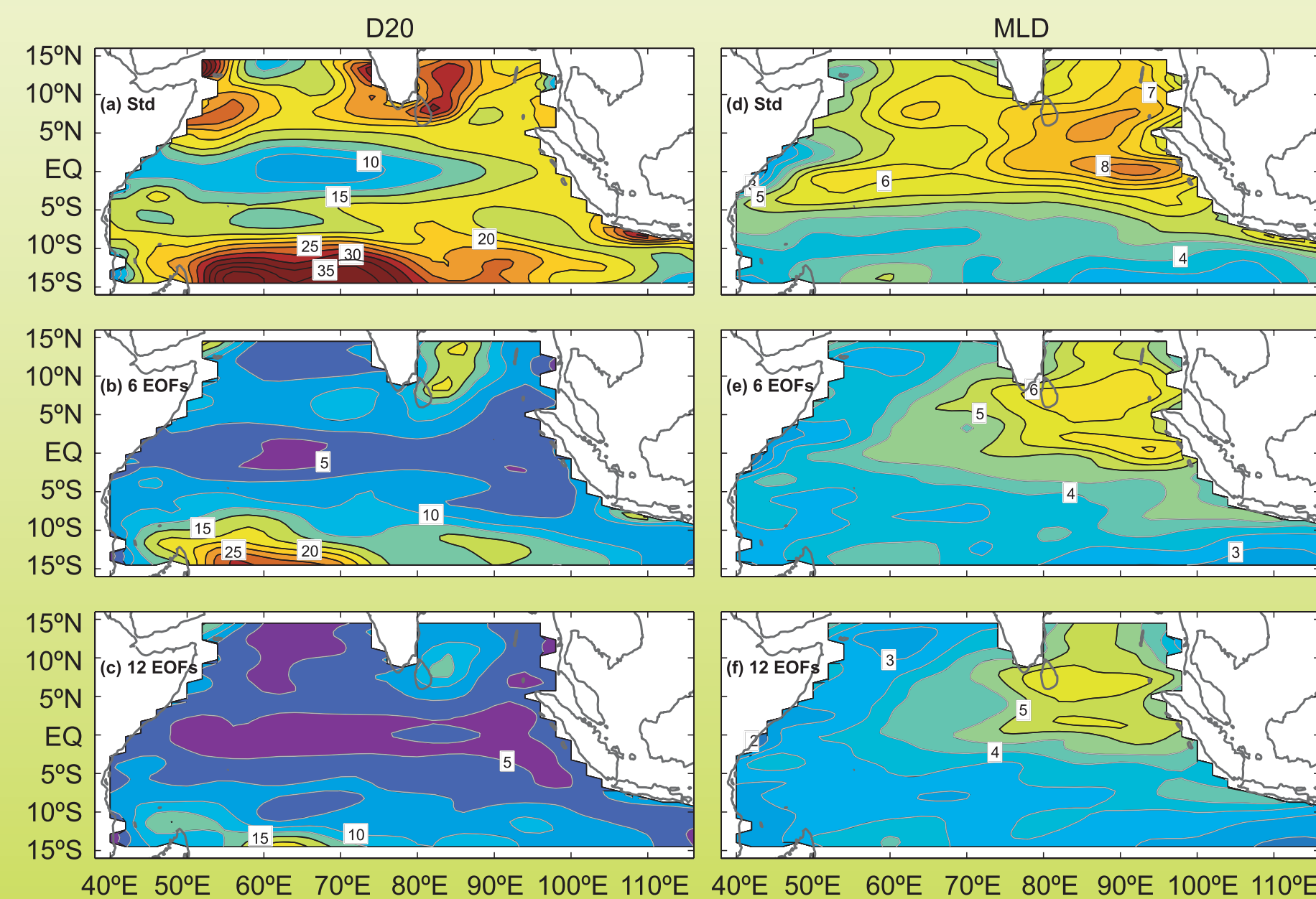


Figure 1 (a,d) Standard deviation of D20 (left) and MLD (right) for years 7-12; and the residuals from the reconstructed fields using (b,e) 6 EOFs and (c,f) 12 EOFs.

PROPOSED

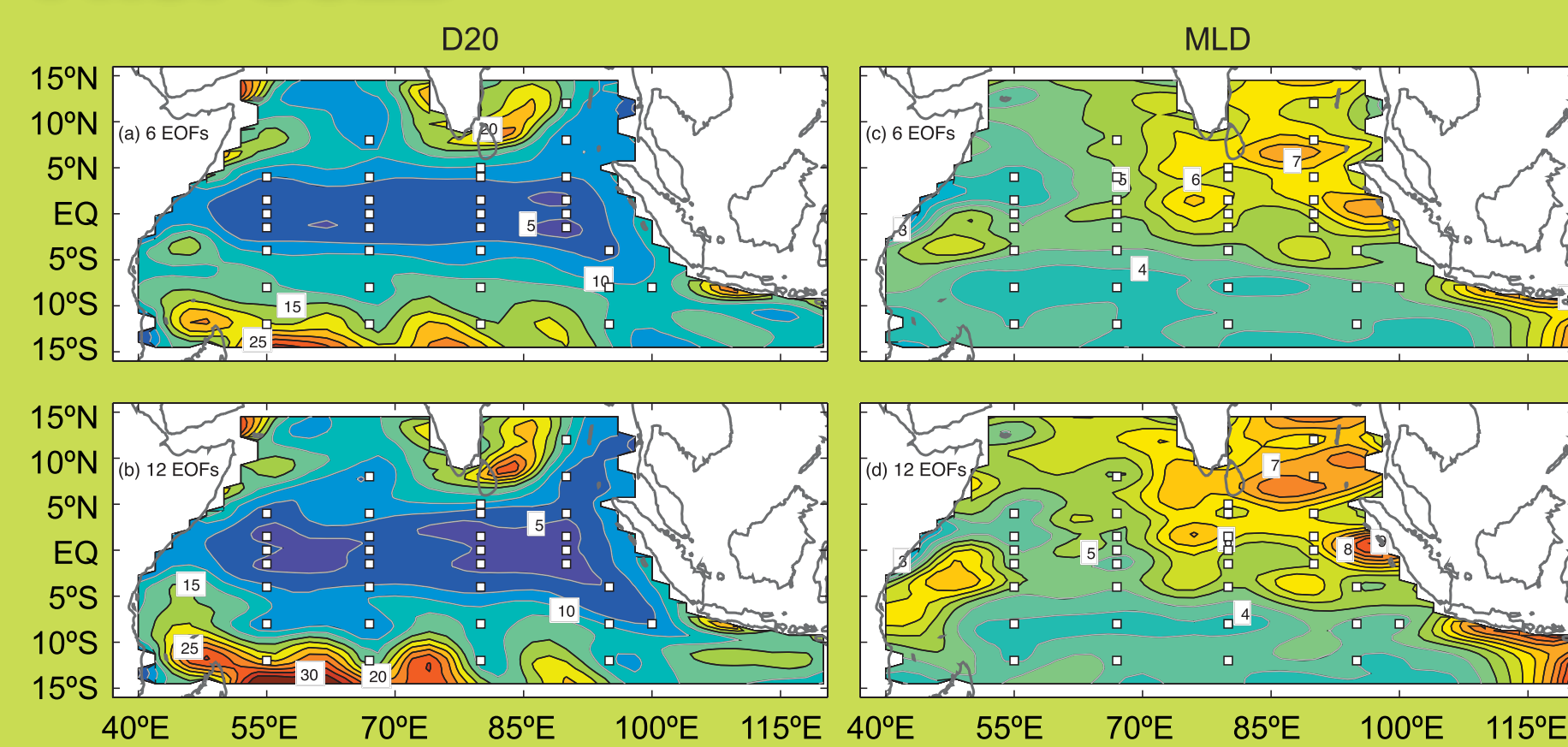


Figure 2 RMSE for D20 (left) and MLD (right) analyses from OSSEs for years 7-12 using (a,c) 6 EOFs and (b,d) 12 EOFs. The observation locations are denoted by the squares.

OPTIMAL

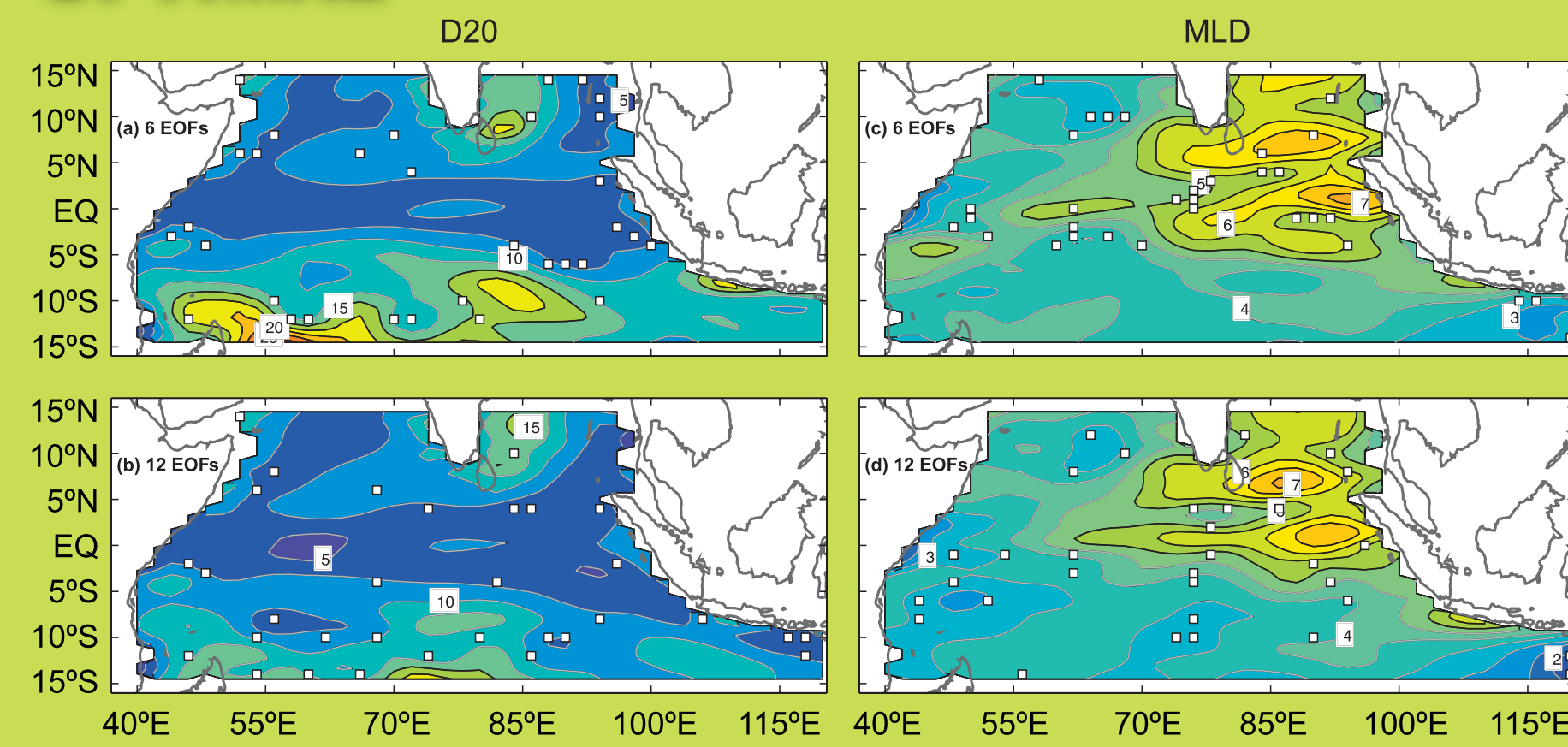


Figure 3 As for Figure 2, except using an optimal array.

CONSOLIDATED

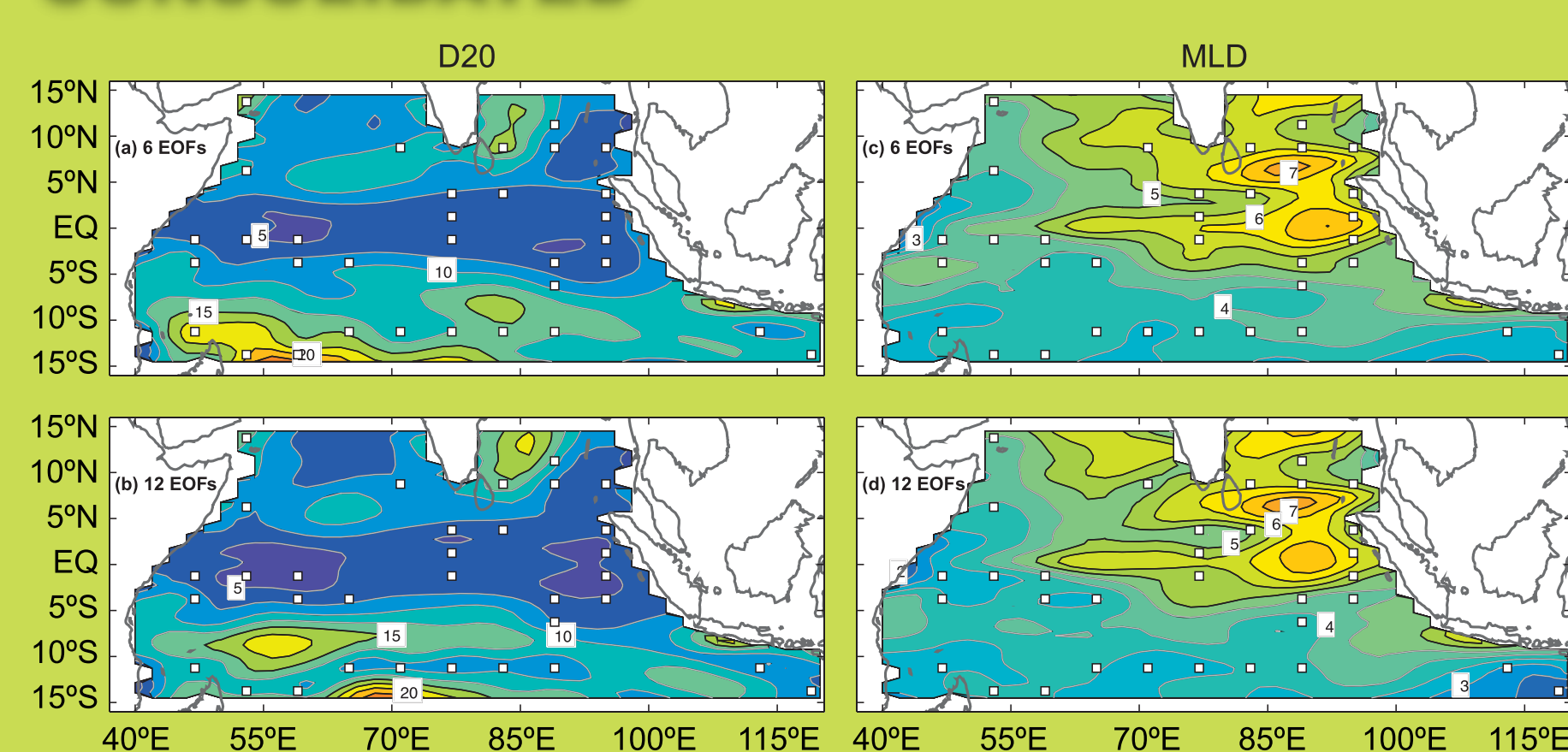


Figure 5 As for Figure 2, except using the consolidated array.

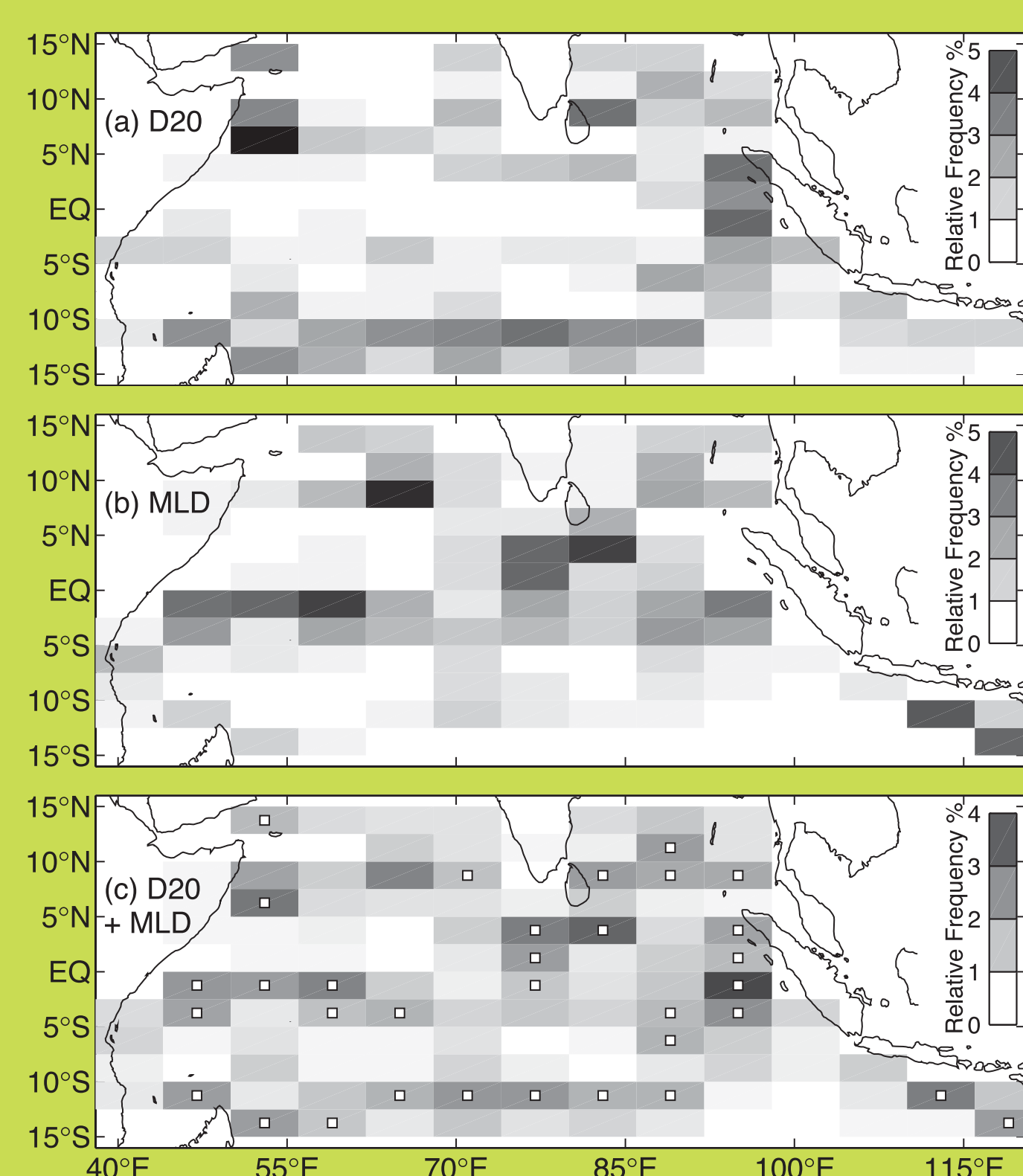


Figure 4 Map of the relative frequency that locations are selected in all OSSEs for (a) D20 and (b) MLD; and (c) both D20 and MLD. The locations of the consolidated array are also plotted in panel (c).

Objective

Through a series of Observing System Simulation Experiments (OSSEs) we seek to design a mooring array for a tropical Indian Ocean mooring array that is suitable for resolving oceanic variability on interannual time scales, represented by the depth of the 20° isotherm (D20), and intraseasonal variability, represented by high-pass filtered mixed layer depth (MLD). ■

Model Configuration

The model is a global configuration of MOM2 with zonal resolution of 2°; meridional resolution of 0.5° near the equator and 1.5° near the poles; and with 25 vertical levels. Following a 20-year spin-up, the model is run for 12 years and is forced by 3-day-averaged wind stress from a blend of NCEP-NCAR fields and FSU climatology; and surface heat and freshwater fluxes derived from an atmospheric boundary layer model with a flux correction. ■

Analysis System and Array Design

A column vector of the analysed model state w is given by

$$w = w^{\text{mean}} + Mc, \quad (1)$$

where w^{mean} is the temporal mean; $M = (w_1^{\text{EOF}} \ w_2^{\text{EOF}} \ \dots \ w_m^{\text{EOF}})$ is a matrix of Empirical Orthogonal Functions (EOFs) and c is a column vector of weighting coefficients that are determined by calculating the least-squares solution to

$$HMc = d, \quad (2)$$

where H is an operator that interpolates from grid-space to observation-space; and d is a vector of observations. The ability of (1-2) to determine the correct weights in c depends on how well the observations project onto the EOFs; and more specifically, how well they distinguish between the different EOFs.

We seek to define H (i.e., the observation locations) so that HM is orthogonal. To achieve this, we apply a procedure that attempts to define H , so that $\text{cond}((HM)^T (HM))$ is minimized (HM is orthogonal if $\text{cond}((HM)^T (HM)) = 1$). Starting with locations at every model grid point, we eliminate the location that, when withheld, gives the smallest $\text{cond}((HM)^T (HM))$. We recursively repeat the procedure until the desired number of locations remain. ■

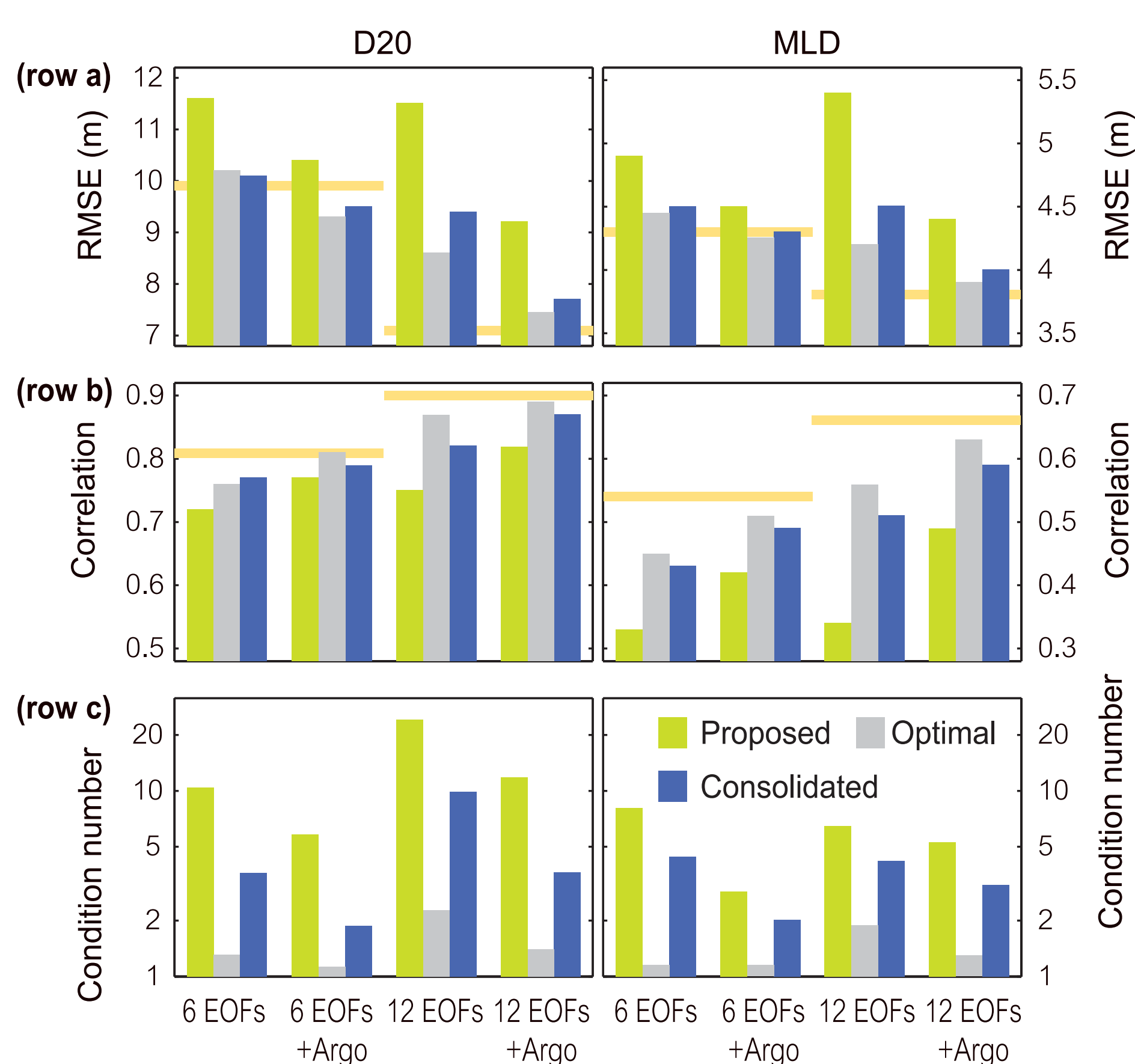


Figure 6 Basin-averaged RMSE (row a) and cross-correlations (row b). The horizontal lines denote the RMS residual (row a) and the cross-correlation (row b) between the raw and reconstructed fields using 6 (left line) and 12 (right line) EOFs for years 1-6 from Figure 1. Row (c) shows $\text{cond}((HM)^T (HM))$ for each OSSE; the vertical axis for row (c) is logarithmic.

Results

We perform a series of OSSEs that produce analyses of D20 and MLD using simulated observations for model years 7-12, using EOFs derived from model years 1-6. For some OSSEs, where it is explicitly stated, we include Argo observations on a uniform 6x6° grid. We compare the true and analysed fields to determine the root-mean-squared error (RMSE) for each OSSE. The expected lower bound for the RMSE using an optimal array is given by the residuals of the reconstructed EOFs using 6 and 12 modes (**Figure 1**). The standard deviations of D20 and MLD are also shown in **Figure 1**.

We compare the RMSE using the proposed array (**Figure 2**) and the optimal array (**Figure 3**) for OSSEs using 6 and 12 EOFs for D20 and MLD. Clearly the optimal arrays outperform the proposed array. However we note that the details of the optimal arrays are quite different for each OSSE. To assess this sensitivity we perform a total of 24 OSSEs (using 3 times series; 6 and 12 EOFs; with and without Argo observations for D20 and MLD). Using observation locations from all OSSEs we construct a map of the relative frequency of optimal locations (**Figure 4**) and construct a consolidated array that represents the general features of the arrays identified by different OSSEs.

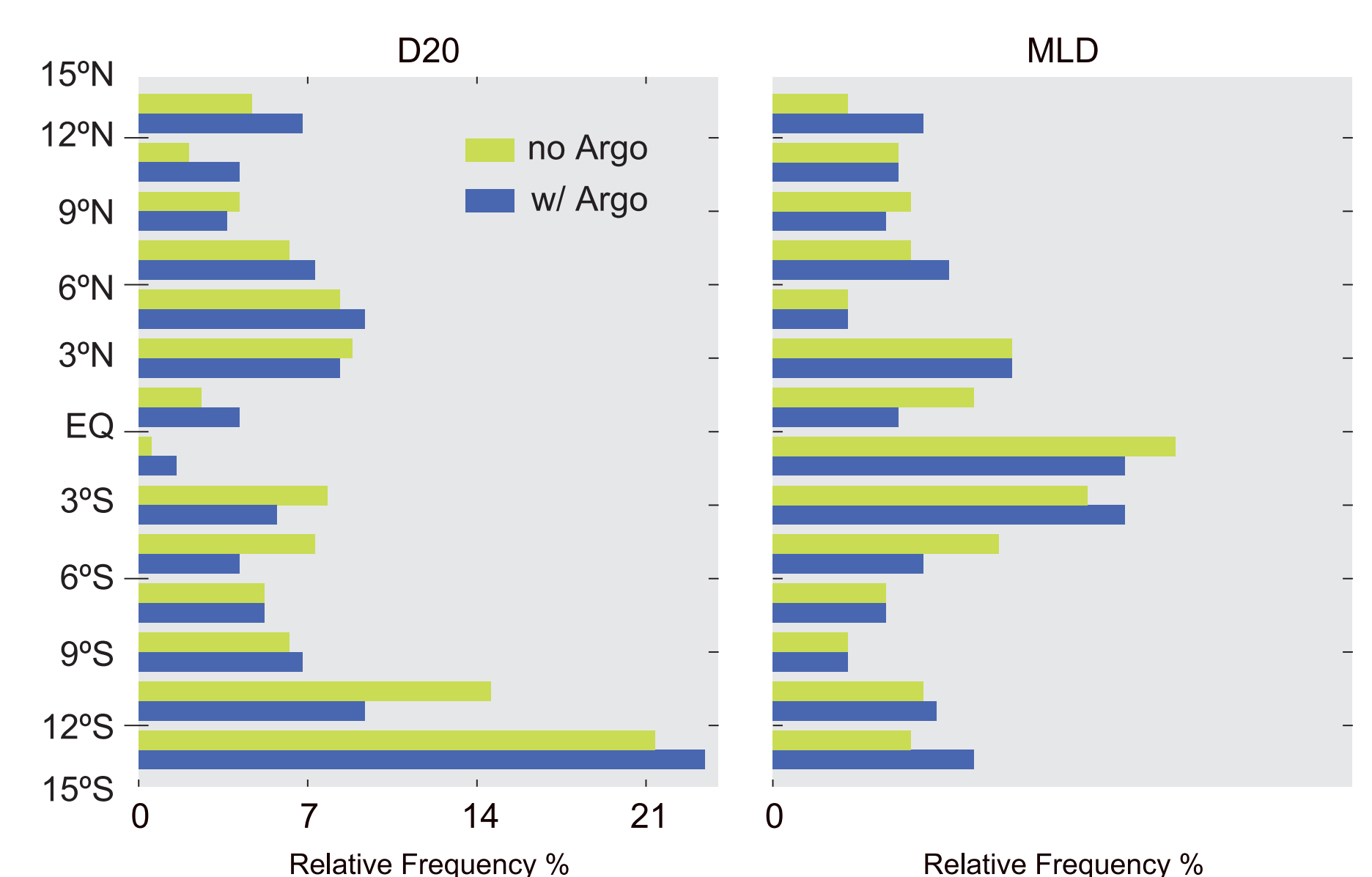


Figure 7 Relative frequency histogram of the meridional distribution of the 33 optimal observation locations for all 24 OSSEs for D20 (left) and MLD (right).

We repeat the OSSEs using the consolidated array (**Figure 5**) and demonstrate that while the consolidated array performs comparably to the optimal array (**Figure 3**); it clearly outperforms the proposed array in all cases (**Figure 2**). This is further illustrated in **Figure 6**, showing the basin averaged cross-correlations and RMSEs for all OSSEs, along with $\text{cond}((HM)^T (HM))$.

The meridional distribution of optimal locations for all OSSEs is shown on the relative frequency histogram in **Figure 7**. This demonstrates the importance of observations south of the equator for interannual variability; and observations along the equator for intraseasonal variability. ■

Conclusions

We find that in general, observations south of 8°S and off the Indonesian coast are most important for resolving interannual variability; while observations a few degrees south of equator, west of 75°E; and a few degrees north of the equator, east of 75°E, are important for resolving intraseasonal variability. ■

